*Desalination and Water Treatment*
www.deswater.com

doi: 10.1080/19443994.2015.1036777

57 (2016) 10443–10450
May

Taylor & Francis
Taylor & Francis Group

# Electrochemical behaviour of the titanium-seawater interface at the Cape-Djinet, Boumerdes thermal station: influence of the potential, temperature, and brine

Naima Ghemmit-Doulache[a,b,*], Ali Remli[a]

[a]*Faculty of Sciences, Chemistry Department, University M'Hamed Bougara of Boumerdes, Boumerdes, Algeria 35000, Algeria, Tel. +213 551134464; Fax: +213 24799334; email: ghe2006dou@gmail.com (N. Ghemmit-Doulache), Tel. +213 775960132; email: remliali2012@gmail.com (A. Remli)*

[b]*Fibrous Polymers Treatment and Forming Laboratory, Faculty of Engineering Science, University M'Hamed Bougara of Boumerdes, Avenue of Independence, Boumerdes, Algeria 35000, Algeria*

Received 13 March 2014; Accepted 24 March 2015

ABSTRACT

Here, we describe the characteristics of the Cape-Djinet thermal station seawaters of Boumerdes (Algeria). The high hardness had disastrous consequences. Potential, temperature and brine effects on calcareous deposition on titanium electrodes were measured using chronoamperometry and are reported in this paper. Electrochemical measurements showed that the dissolved oxygen played a key role in calcareous deposition. It has been shown that the reaction of reduction oxygen dissolved on the titanium electrode occurred with a global 4 electron process. Scanning electron microscopy images of titanium electrodes that were polarized at −1.3 V/SCE for 1 hour in natural seawater at 20°C showed that the electrode surface was completely covered with deposits in the form of compact layers that were adherent to the surface of the electrode followed by well-dispersed crystals. SDE analysis confirmed these results in which the peaks were rich in magnesium, oxygen and calcium. In contrast, for the brine solution, the deposit was in the form of crackled, weakly bonded platelets followed by those with a small crystal grain size having cubic form. SDE analysis revealed that these crystals were strongly related to sodium chloride salt.

*Keywords:* Natural seawater; Titanium; Potential; Temperature; Brine

## 1. Introduction

Scale formation problems threaten many industrial activities. In general, the exploitation of the Cape-Djinet circuit seawater desalination thermal plant (located on the east sea of Algiers, near the city of Cape-Djinet in the town of Boumerdes (Algeria)) faces three types of problems: biological developments, scaling and corrosion. Under certain conditions, these three problems interact with each other to form hard deposits that are highly adherent to the walls of tubes [1].

During the heating of seawater, hardened salts tend to come off. This fallout deposited on interior surfaces of tubes and heat exchangers forms a hard crust and causes an increase in power consumption and lower performance, which may limit their operation [2]. The objective of this study fits into this framework. Indeed, we followed the evolution of the recovery of titanium

*Corresponding author.

electrodes by calcareous deposit depending on the potential, temperature and brine using voltammetry (linear and cyclic) and chronoamperometry.

Electrochemical methods consist of determining calcareous deposit formation on titanium electrodes by the dissolved oxygen reduction [3,4]:

$$O_2 + 2H_2O + 4\grave{e} \longrightarrow 4OH^-$$

$$O_2 + 2H_2O + 4\grave{e} \longrightarrow 4OH^- \quad (1)$$

and/or by the water reduction:

$$2H_2O + 2\grave{e} \longrightarrow H_2 + 2OH^- \quad (2)$$

The production of hydroxyl ions ($OH^-$) by reactions (1) and (2) allows magnesium hydroxide precipitation, provided that the interfacial pH reaches the critical value of 9.3 [4]:

$$Mg^{2+} + 2OH^- \rightarrow Mg(OH)_2(s) \quad (3)$$

Moreover, these reactions lead to changes in the inorganic carbonic equilibrium at the metallic interface:

$$OH^- + HCO_3^- \rightarrow H_2O + CO_3^{2-} \quad (4)$$

and allow $CaCO_3$ precipitation:

$$Ca^{2+} + CO_3^{2-} \rightarrow CaCO_3(s) \quad (5)$$

In our case, to have additional information that allows us to better understand the mechanisms of calcareous deposit formation ($CaCO_3$ and $Mg(OH)_2$) [5,6], we used two techniques: voltammetry and chronoamperometry. The first technique consists of imposing on titanium electrode, as the working electrode, a potential that varies linearly. The measurement of current intensity that flows between the working electrode and the counter electrode allows one to obtain polarization curves ($I = f(E)$), which inform us of the electrochemical behaviour of titanium/solution interface.

The potential scan rate and the electrode nature influence the position and the shape of the polarization curve. The reaction rate is governed by a diffusion step in which the rotation speed of the electrode is constant, the diffusion-limited current $i_d$ becomes maximum if Cs ($x = 0$) = 0.

Admitting the validity of the Nernst hypothesis, the reaction rate is written as [7]:

$$\frac{i}{nF} = \frac{-DC_\infty}{\delta} \quad (6)$$

In laminar flow, the diffusion layer thickness value is:

$$\delta = 1.61 D^{1/3} v^{1/6} W^{-1/2} \quad (7)$$

The corresponding value of the current is called the "diffusion limited current", which appears on the polarization curve as a diffusional plateau. The diffusion-limited current from the Levich equation is proportional to the square root of the electrode rotation speed.

$$I_L = 0.62 n F A D_{O2}^{2/3} v^{-1/6} C_\infty W^{1/2} = K W^{1/2} \quad (8)$$

where $I_L$ is the limiting current in $A$, $n$ is the number of electrons involved in electrode reaction, $F$ is Faraday's constant (96,485 C $mol^{-1}$), $A$ is the electrode area in $cm^2$, $D_{O2}$ is the oxygen diffusion coefficient in the electrolyte in $cm^2\ s^{-1}$, $v$ is the kinematic viscosity of the electrolyte in $cm^2\ s^{-1}$, $C_\infty$ is the concentration of oxygen in the bulk solution in mol $cm^{-3}$, $W$ is the angular speed of the rotating disc electrode in rad $s^{-1}$ (1 rpm = $2\pi/60$ rad $s^{-1}$) and $K$ is the constant of the Levich criterion (A $cm^{-2}$ $rad^{-1/2}$ $s^{1/2}$).

The Levich equation is valid only if the rotating speed is important to rapidly reach steady state while remaining in a laminar flow [8].

## 2. Experimental

### 2.1. Set-up

Electrochemical measurements were carried out using a programmable electrochemical system and an analytical radiometer (PGP 201) France, which were driven by a Voltmaster 4 to save the polarization curves ($I = f(E)$) and chronoamperometric curves ($I = f(t)$). The working electrode was connected to a rotating system (speed control unit), and we manually monitored its rotation speed.

The working electrode in titanium had an active area of 7.06 $mm^2$, in which a calcareous deposit was formed at different potential values for two hours compared with a saturated calomel electrode (SCE) as Refs. [9–12]. The titanium electrode was polished on abrasive paper in silicon carbide (SiC 1,200) (14 μm). Then, the electrode was placed in a diluted hydrochloric acid solution, in acetone for 10 min, and then in 40% ethylic alcohol for 15 min. The electrode was then rinsed with Milli-Q water. To reduce the oxide layer,

which formed with exposure to fresh air on the titanium surface, electrochemical polishing was necessary to render a smoother and brighter surface on the titanium. The procedure is described in Refs. [13,14]. To this end, the electrode was polarized at −2.5 V/SCE for 5 min and was polarized at an imposed potential.

### 2.2. Cape-Djinet seawater characterization

The natural seawater (NSW) came from the Cape-Djinet thermal desalination plant. This water was of considerable salinity, charged with calcium and magnesium (see Table 1).

## 3. Results and discussions

### 3.1. Linear voltammetry

#### 3.1.1. Speed rotation electrode effect

Because dissolved oxygen reduction is the main driving force of electrochemical scaling, we plotted the polarization curves ($I = f(E)$) in the cathodic domain. Fig. 1 shows the polarization curves ($I = f(E)$) obtained in NSW (composition specified in Table 1) at different rotation speeds of titanium. The scanning was performed from 0 to −2 V/SCE at 20°C with a scan rate of 10 mV/SCE.

By examining the curves, we found that they had a wave that ran from −0.6 to −1.5 V/SCE with a global 4 electron process, which corresponded to the reduction of the dissolved oxygen reaction (1). In this case, the direct reduction of $O_2$ to $OH^-$ predominated followed by the reduction in $O_2$ to $H_2O_2$ and then $H_2O_2$ to $OH^-$, which was related to the nature of the metal:

$$O_2 + 2H_2O + 2\grave{e} \longrightarrow H_2O_2 + 2OH^- \quad (9)$$

$$H_2O_2 + 2\grave{e} \longrightarrow 2OH^- \quad (10)$$

Table 1
NSW characterization at 20°C

| Analysis | Value |
|---|---|
| pH | 7.6 |
| Electrical conductivity (Cd) | 51.6 ms/cm |
| Total hardness (TH) | 660 °F |
| Calcium Hardness ($TH_{Ca}^{2+}$) | 300 °F |
| Magnesium hardness ($TH_{Mg}^{2+}$) | 360 °F |
| Alkalimetric title (TA) | 0.85 °F |
| Complete alkalimetric title (TAC) | 11.5 °F |

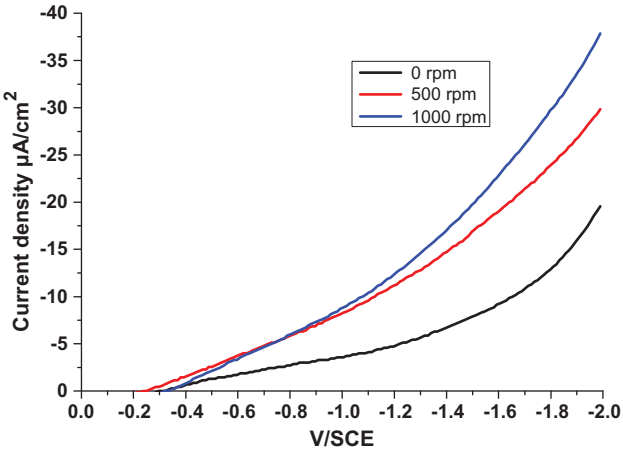


Fig. 1. Polarization curves ($I = f(E)$) of NSW–titanium electrodes with different rotation speeds at 20°C.

Beyond a potential of −1.5 V/SCE, we found a strong hydrogen evolution resulting from the water reduction reaction (2).

#### 3.1.2. Temperature effect

Fig. 2 shows that the current increase was proportional to the temperature increase. In fact, the temperature increase produced two effects. On one hand, it favoured water reduction. On the other hand, it produced an increase in the limiting current of dissolved oxygen reduction, which was linked to the increase of the oxygen diffusion coefficient. This parameter was demonstrated to be more important than the opposite effect, which was the reduction of oxygen solubility in

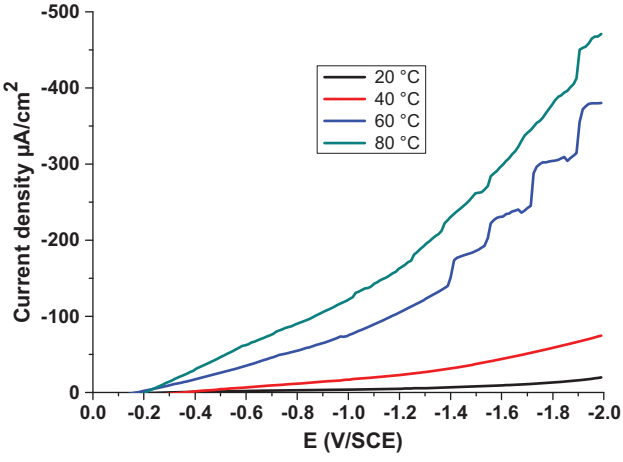


Fig. 2. Polarization curves ($I = f(E)$) of NSW–titanium electrodes for different temperatures at 500 rpm.

water, as Rosset already showed [15]. Indeed, Kunjapur et al. [16] showed that the $O_2$ reduction reaction was accelerated by a temperature increase. However, Ketrane et al. [17,18] noted that for electrochemical scaling tests in temperature range of 20–50°C, the potential ($E$) of −1.0 V/SCE seemed adequate. At this potential, for all temperatures, the oxygen reaction sufficiently developed to provide interfacial pH conditions for precipitation. Moreover, for these conditions, hydrogen gas evolution was not very developed. The increase in the currents was explained by the thermal agitation effect and by two other combined effects: the decrease of the solution viscosity and the increase in the diffusion coefficient [4,19].

### 3.2. Cyclic voltammetry

#### 3.2.1. Speed rotation electrode effect

Fig. 3 shows the voltammograms registered in NSW at scan rate of 10 mV/s, we obtain:

When scanning towards cathodic potentials, a diffusion plateau appeared ranging from −0.6 to −1.5 V/SCE in an overall four-electron process. This plateau increases with increase of the electrode rotation speed.

During the return scan towards anodic potentials, a peak appeared corresponding to the oxidation of titanium formed by titanium oxide ($E_a$ = +1.0 V/SCE).

#### 3.2.2. Temperature effect

In Fig. 4, we noticed that the increase in current density was proportional to the temperature.

When scanning towards cathodic potentials, the temperature increase had two effects: it favoured the water reduction and produced an increase in the current limit of dissolved oxygen reduction. The shape of the curve was similar to those in Fig. 2 and was in conformity with what has been reported in the literature [20]. A diffusion stage relationship to the dissolved oxygen reduction was observed. $OH^-$ ions resulted from cathodic reduction of the dissolved oxygen in water (Eq. (1)). At more cathodic polarization, an intense hydrogen release due to the water decomposition reaction (Eq. (2)) was observed.

When scanning towards anodic potentials, the increase in temperature accelerated the oxidation of titanium.

### 3.3. Chronoamperometry

#### 3.3.1. Potential effect

Under the same experimental conditions (temperature 20°C, electrode rotation speed 1,000 rpm and NSW solution), we varied the potential imposed on the working electrode from −0.8 to −1.4 V/SCE. By examining the curves in Fig. 5, we used the parameters summarized in Table 2. Through analysis of these parameters, we could deduce that a calcareous deposit was supported for the more cathodic potentials. Indeed, the lowest scaling time ($t_S$) corresponded to the deposit realized at −1.4 V/SCE ($t_S$ = 11 min). This time scaling was inversely proportional to the applied cathodic potential contrary to the index scaling ($I_S$) defined by $I_S = 1{,}000/t_S$. This result was in accordance with the results of work already reported [21,22]. Additionally, an increase in the initial current ($I_0$) vs.

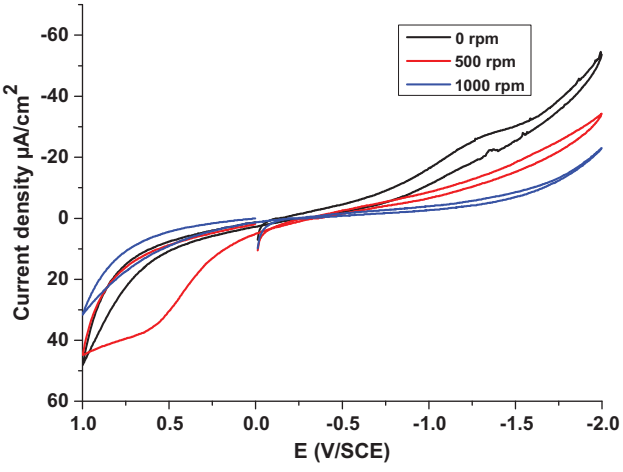


Fig. 3. Cyclic voltammograms of the NSW–titanium interface at 20°C for different rotation speeds.

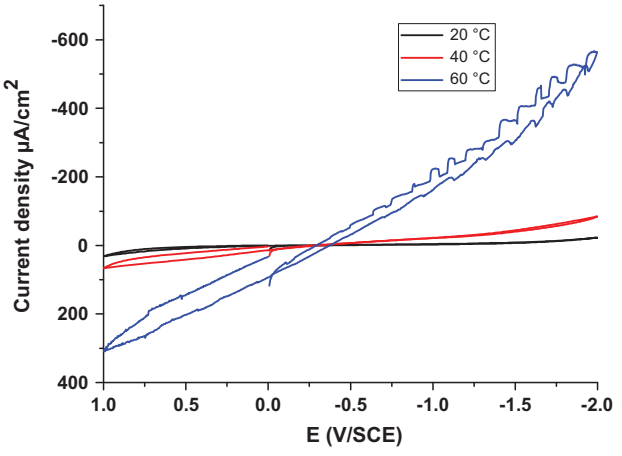


Fig. 4. Cyclic voltammograms of the NSW–titanium interface at 500 rpm at different temperatures.

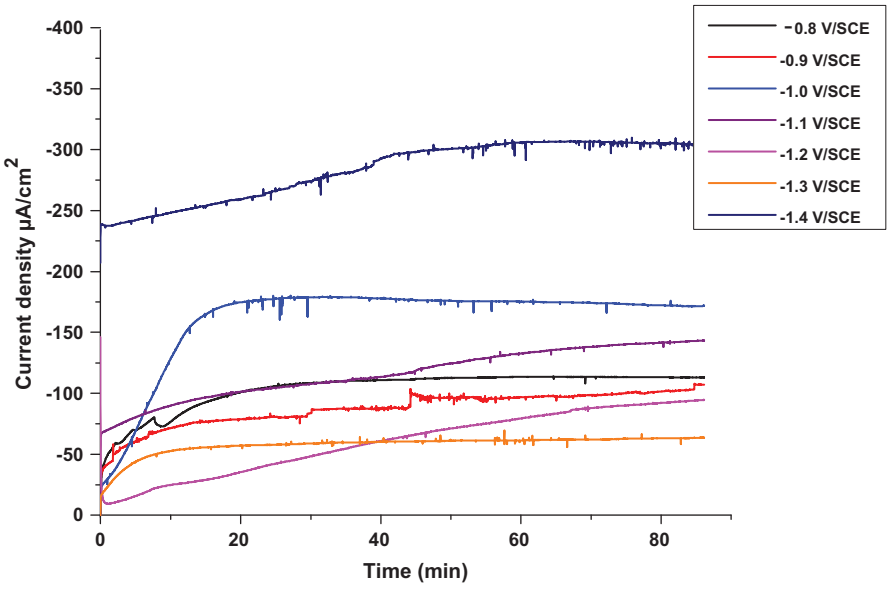


Fig. 5. Chronoamperometric curves of the NSW–titanium interface at 1,000 rpm and at 20°C under different potentials.

Table 2
Parameters determined from the chronoamperometric curves

| $E$ (V/SCE) | −0.8 | −0.9 | −1.0 | −1.1 | −1.2 | −1.3 | −1.4 |
|---|---|---|---|---|---|---|---|
| $I_0$ (µA/cm$^2$) | −5.71 | −23.28 | −15.42 | −63.00 | −51.57 | −16.14 | −207.00 |
| $I_{res}$ (µA/cm$^2$) | −113.14 | −107.14 | −171.85 | −143.28 | −94.57 | −63.42 | −304.14 |
| $t_S$ (min) | 30 | 20 | 18 | 15 | 14 | 12 | 11 |
| $I_S$ (min$^{-1}$) | 33.33 | 50.00 | 55.55 | 66.66 | 71.42 | 83.33 | 90.90 |

potential imposed confirmed that germination was faster at more cathodic potentials.

The scaling indices were in the range of $15 < I_S > 100$, which indicated that NSW calcified as classified by Ledion et al. [23].

The deposit formed at −1.4 V/SCE weakly adhered to the surface of the electrode and could be easily removed by slight mechanical friction. This result was explained by friability of the deposit caused by strong hydrogen evolution where the highest residual current corresponded to the potential ($i_{res}$ = −304.143 µA/cm$^2$) and high concentration of sodium chloride (29.631 g/L).

### 3.3.2. Temperature effect

Fig. 6 shows the chronoamperometric curves at different temperatures, 20, 40, 60 and 80°C. The tests were carried out to a potential of −1.3 V/SCE and a speed rotation of 1,000 rpm for one hour.

In reviewing these curves, we found that the parameters already mentioned above ($t_S$ and $i_{res}$) were inversely proportional to the temperature at lower

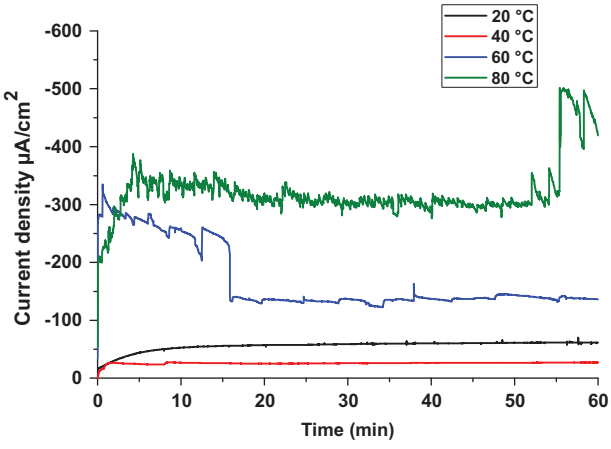


Fig. 6. Chronoamperometric curves of NSW–titanium interfaces at 1,000 rpm and at −1.3 V/SCE at different temperatures.

values at 40°C. However, we noticed that $t_S$ and $i_{res}$ increased.

We observed that at $t$ = 0 min, when the temperature increased, the current density became high,

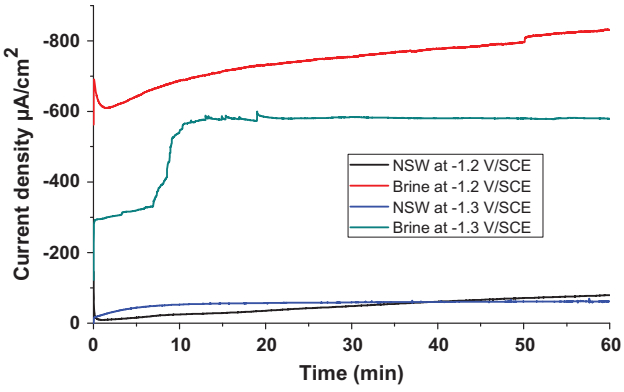


Fig. 7. Brine effect on calcareous deposition obtained in NSW at 1,000 rpm under different potentials.

indicating that deposition was quick. Additionally, we noticed that the current decrease was very fast, revealing the important calcareous deposition. Furthermore, we observed fluctuations in the curves at 60 and 80°C, showing the friability and the porosity of layer deposit formed. This result was caused by the strong hydrogen evolution and the change of the deposit structure at high temperatures together with the influence of chlorides where the residual current increased as a function of temperature. Indeed, the temperature increase had two effects. Firstly, it promoted water reduction, inducing an important hydrogen current. Secondly, it produced an increase in limiting oxygen reduction related to an increase of the diffusion coefficient of dissolved oxygen. Following these two effects, an increase in the interfacial pH led to the formation of brucite. In other words, the temperature increase accelerated water reduction; therefore, the interfacial pH increased, thereby favouring the formation of Mg $(OH)_2$. However, the acceleration of water reduction produced a significant hydrogen evolution, and the transfer did not follow a diffusion regime.

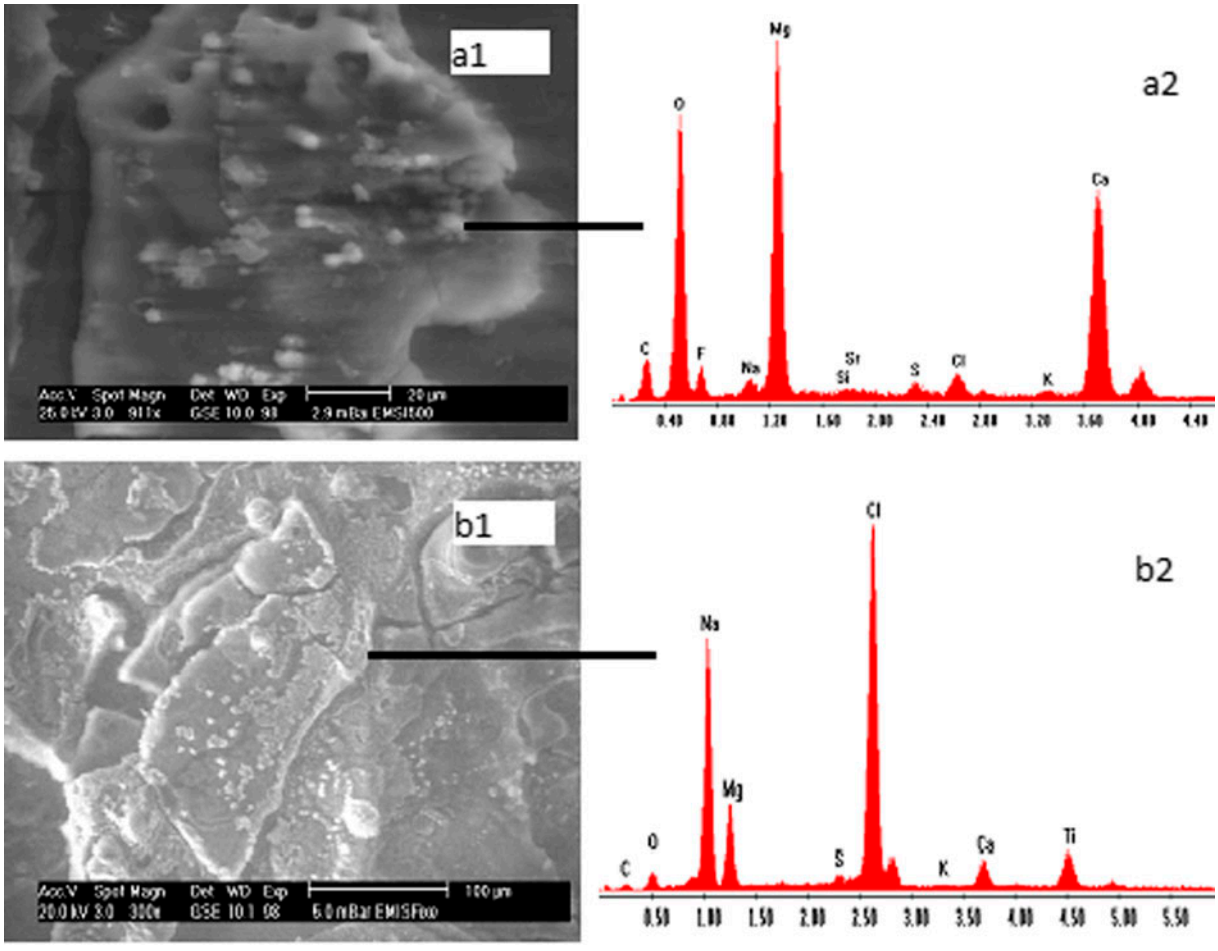


Fig. 8. Microscopic observations of calcareous deposits at −1.3 V/SCE, (a1) NSW, (b1) brine, (a2) and (b2) SDE spectra of the indexed zones.

#### 3.3.3. Brine effect

Seawater is known for its high salinity and power lime scale. In addition, the evaporation of seawater in the heat exchanger circuit desalination part entails a significant increase in salinity. Then, it becomes interesting to explore the effect of salinity on the scale formation phenomenon. Chloride ions were chosen because they are known to have a low activity in the calcareous deposition phenomenon [24].

Fig. 7 shows curves for the variation of the current density vs. time for NSW and brine solutions to −1.2 and −1.3 V/SCE, respectively. These curves showed that brine played a significant role in calcareous deposition. Indeed, brine entailed a high current density and higher residual current than that of NSW, which was explained by the friability of the deposit caused by a high concentration of sodium chloride (32.20 g/L NaCl).

### 3.4. Morphological analysis and chemical composition

Scanning electron microscopy images of titanium electrodes polarized at −1.3 V/SCE for 1 hour in NSW and in brine at 20˚C are given in Fig. 8. Fig. 8(a1), which is related to seawater, shows that the electrode surface was completely covered with deposit in the form of compact layers that were adherent to the electrode surface, followed by well-dispersed crystals [25]. These results were in agreement with those found by chronoamperometry. Indeed, calcareous deposits gradually overlaid the metal surface and insulated the metal phase of water, which caused a decrease in the reduction current of oxygen through the electrode (see Fig. 7). Consequently, the residual current was directly related to the morphology of the deposit; the latter was more compact and more insulating when the residual current was low. Additionally, cracking of the deposit observed on Fig. 8(a1) was caused by hydrogen bubbles that formed at the lower potential at −1.1 V/SCE [5,26,27]. Indeed, the potential was sufficiently negative to yield the water reduction, and thereby significantly increase the interfacial pH. The SDE analysis confirmed these results in which Fig. 8(a2) shows peaks rich in magnesium, oxygen and calcium. This result agreed with those of authors [5,28,29] who have found that predominant allotropic forms of calcareous deposits (formed at −1.3 V/SCE) were brucite $Mg(OH)_2$ and aragonite $CaCO_3$.

In contrast, Fig. 8(b1) of brine shows that the electrode surface was completely covered with a deposit formed of weakly bonded, crackled platelets followed by those that had a small crystal grain size and were cubic shaped. The SDE analysis (Fig. 8(b2)) revealed that these crystals were strongly related to sodium chloride salt, as noted above.

## 4. Conclusion

In this work, the effects of the potential, temperature and brine on calcareous deposition on a titanium surface were investigated. Chronoamperometric measurements and surface analysis showed that the deposit realized at a potential of −1.3 V/SCE was formed by compact layers and was adherent to the electrode surface. The effect of brine on calcareous deposition showed that the electrode surface was covered with crackled platelets composed of sodium chloride. These results agreed with the chronoamperometric measurements, showing that the current density and the residual current were more important than those of seawater. The same result was observed at high temperature in which we obtained fluctuations in the curves at 60 and 80˚C, revealing the friability and porosity of the layer deposit formed.

Future work will aim to study the effects of different inhibitors on calcareous deposition on titanium surfaces.

## References

[1] D.P. Logan, S.P. Rey. Scale control in multiple stage flash evaporators, NACE. Corrosion/'85, paper 360 or Mat. Perf. 25 (1987) 38–44.
[2] B.B. Balvet, J.H. Davidson, Seawater circuits treatments and materials, De Chambre syndicale de la recherche et de la production du pétrole et du gaz naturel, Comité des techniciens, Technip (1998) 3–21.
[3] C. Deslouis, D. Festy, O. Gil, G. Rius, S. Touzain, B. Tribollet, Characterization of calcareous deposits in artificial seawater by impedance techniques. I—Deposit of $CaCO_3$ without $Mg(OH)_2$, Electrochim. Acta 43 (1998) 1891–1901.
[4] C. Deslouis, D. Festy, O. Gil, V. Maillot, S. Touzain, B. Tribollet, Characterization of calcareous deposits in artificial seawater by impedances techniques. II—Deposit of $Mg(OH)_2$ without $CaCO_3$, Electrochim. Acta 45 (2000) 1837–1845.
[5] Ch. Barchiche, C. Deslouis, D. Festy, O. Gil, Ph. Refait, S. Touzain, B. Tribollet, Characterization of calcareous deposits in artificial seawater by impedance techniques. III—Deposit of $CaCO_3$ in the presence of Mg(II), Electrochim. Acta 48 (2003) 1645–1654.
[6] T. Chen, A. Neville, M. Yuan, Assessing the effect of $Mg^{2+}$ on $CaCO_3$ on scale formation–bulk precipitation and surface deposition, J. Cryst. Growth 275 (2005) e1341–e1347.
[7] A.J. Bard, L.R. Faulkner, Methods forced convection. in: C.M.A. Brett, A.M.O. Brett (Eds.), Electrochemistry: Principles, New York, Methods and Applications, Oxford University Press, 1983, pp. 313–333.

[8] V. Filinovsky, Y. Pleskov, Rotating disk and ring electrodes in investigations of surface phenomena at the metal-electrolyte surface, in: D.A. Cadenhead, J. Danielli (Eds.), Progress in Surface and Membrane Science, vol. 10, Academic Press, London, 1976, pp. 27–101.
[9] N. Ghemmit-Doulache, Kinetic Study of Calcareous Deposit on Titanium Electrode and Scaling Mechanism, Comparing the Chemical and Electrochemical Method, Doctoral Thesis, University M'Hamed Bougara of Boumerdes, Algeria, 2011.
[10] N. Ghemmit-Doulache, H. Khireddine, D. Si, Salah, verification of Levich law-determination of hydrogen currents during calcareous deposition, J. Environ. Sci. Eng. 5 (2011) 1269–1275.
[11] N. Ghemmit-Doulache, H. Khireddine, M. Bourouina, N. Boudissa, Study of the antideposit effect of 2-hydroxy-4-methylbenzylphosphonic acid, Asian J. Chem. 21 (2009) 2270–2282.
[12] M. Bourouina, S. Bourouina-Bacha, D. Hadiouche, Electrochemical study of the inhibition for scaling deposition in seawater, Technologies de Laboratoire (Lab. Technol.) 6 (2011) 115–120.
[13] L. Beaunier, C. Gabrielli, G. Poindessous, G. Maurin, R. Rosset, Investigation of electrochemical calcareous scaling, J. Electroanal. Chem. 501 (2001) 41–53.
[14] SFC Flash News 2004 N°23 15. Available from: <http://www.sfc.fr/FFC.JPG>.
[15] R. Rosset, Physical processes antiscalling: myth or reality? L'actualité chimique (Chemical News), January/February (1992) 125–148.
[16] M.M. Kunjapur, W.H. Hartt, S.W. Smith, Influence of temperature and exposure time upon calcareous deposits, Corrosion 43 (1987) 674–679.
[17] R. Ketrane, L. Leleyter, F. Baraud, O. Gil, B. Saidani, Effect of temperature and potential on the hydrogen currents during the deposition of tartar electrochemically, in: Proceedings of the 12th National Symposium of Research in IUT, Brest, 1–2 June, 2006.
[18] R. Ketrane, B. Saidani, O. Gil, L. Leleyter, F. Baraud, Efficiency of five scale inhibitors on calcium carbonate precipitation from hard water: Effect of temperature and concentration, Desalination 249 (2009) 1397–1404.
[19] C. Deslouis, A. Doncescu, D. Festy, O. Gil, V. Maillot, S. Touzain, B. Tribollet, Kinetics and characterisation of calcareous deposits under cathodic protection in natural sea water, Mater. Sci. Forum 289–292 (1998) 1163–1180.
[20] G. Poindessous, Study of the Germination Growth of Calcium Carbonate Electrochemically—Influence of the Oxygen Content and Material Transport, Doctoral Thesis, University Paris VI, France, 1998.
[21] S. Tauzain, Study of Calcareous Deposits Structure Formed in the Presence of Flow: Application to Cathodic Protection in Marine, Doctoral Thesis, University Louisiana Rochelle, France, 1997.
[22] N. Ghemmit, Characterization of Scaling Capacity of Seawater, Study of the Effect Antideposit of Acid 2-Hydroxy, 4-Methyl, Benzyl, Phosphonic by Chronoamperometry, Complex Impedance and MEB, Master's Thesis, University M'Hamed Bougara of Boumerdes, Algeria, 2003.
[23] J. Ledion, P. Leroy, J.P. Labbé, Determination of encrusting nature of water by accelerated scaling test, TSM-Water, July/August (1985) 323–328.
[24] H. El Fil, H. Roques, Contribution to the study of scaling phenomena by geothermal water. Part I: Study of the phenomenon onsite and comparison with the pure calcocarbonic system. J. Soc. Chem. Tunisie 4 (2001) 1079–1093.
[25] A. Neville, A.P. Morizot, A combined bulk chemistry/electrochemical approach to study the precipitation, deposition and inhibition of $CaCO_3$, Chem. Eng. Sci. 55 (2000) 4737–4743.
[26] S.L. Wolfson, W.H. Hartt, An initial investigation of calcareous deposits upon cathodic steel surfaces in sea water, Corrosion 37 (1981) 70–76.
[27] J.S. Luo, R.U. Lee, T.Y. Chen, W.H. Hartt, S.W. Smith, Formation of calcareous deposits under different modes of cathodic polarization, Corrosion 47 (1991) 189–196.
[28] G. Phillipponneau, Influence of Various Factors (Calcareous Deposit, Presence of Sulfide, $H_2S$ or $HS^-$, Copper Content) on Electrochemical Behaviors and Mechanical Low Alloy Steels, Cathodically Polarized or Non-Marine Type of Environment, Doctoral Thesis, Research Center of the Central School of Arts and Manufactures in Paris, France, 1982.
[29] O. Gil, P. Refait, J.B. Memet, L. Seguy, Study of calcareous deposits formed during steel cathodic protection: natural deposits and deposits prepared in the laboratory, Europ. J. Hydrol. 31 (2000) 167–182.